Effect of Concentration on the Supramolecular Polymerization Mechanism via Implicit-Solvent Coarse-Grained Simulations of Water-Soluble 1,3,5-Benzenetricarboxamide

Effect of Concentration on Supramolecular Polymerization Mechanism via Implicit Solvent Coarse-Grained Simulations of Water-Soluble 1,3,5-benzenetricarboxamide

*Davide Bochicchio and Giovanni M. Pavan**

Department of Innovative Technologies, University of Applied Sciences and Arts of Southern Switzerland, Galleria 2, Via Cantonale 2c, CH-6928 Manno, Switzerland

giovanni.pavan@supsi.ch

ABSTRACT We report an accurate implicit-solvent coarse-grained model for a water-soluble 1,3,5-benzenetricarboxamide (BTA) supramolecular polymer. The technical advances guaranteed by this CG model allow simulating the self-assembly of a thousand BTA monomers, and easy variation of the BTA concentration into the system down to experimental dilute conditions. In this way, we can monitor the mechanism of supramolecular polymerization as a function of the concentration at submolecular resolution. While increasing the concentration produces rapid formation of large disordered clusters that are then converted into BTA fibers, moving to very dilute concentrations favors early ordering of the oligomers in solution even at small sizes. Interestingly, we observe that below a certain concentration the oligomers that dynamically grow in solution during the self-assembly present the same level (and amplification) of order of pre-stacked equilibrated oligomers of the same size, meaning that concentration-dependent kinetic effects have disappeared from the polymerization mechanism.

TOC GRAPHICS

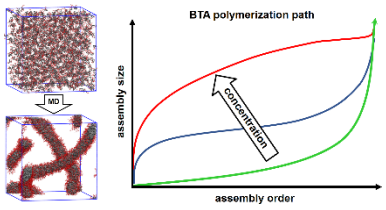

KEYWORDS Supramolecular polymer, self-assembly, implicit-solvent coarse-grained simulation, dry MARTINI, 1,3,5-benzenetricarboxamide (BTA), concentration effect, cooperativity, order amplification

Water-soluble supramolecular polymers, formed via 1D self-assembly of monomers that interact via non-covalent interactions, are attracting increasing attention due to their interesting bioinspired properties.[1–4] Thanks to their supramolecular character these structures possess dynamic properties[5–7] such as self-healing behavior, adaptivity and stimuli responsiveness similar to many natural materials.[8–11] However, while obtaining high-resolution details of how supramolecular polymers polymerize/depolymerize in aqueous environments is a key step toward the rational design of innovative materials for a wide range of bio- and nano-applications,[1–4,9,12,13] this is experimentally difficult, if not prohibitive, due the small size of the monomers and their dynamic behavior.

Among many others,[4,14–18] 1,3,5-benzenetricarboxamide (BTA)-based supramolecular polymers are ideally suited for fundamental studies on supramolecular polymerization[19] and well-studied also in water.[20–22] BTA monomers self-assemble due to core stacking and three-fold hydrogen-bonding between the amides surrounding the aromatic cores.[19] While supramolecular BTA polymerization has been well-studied in organic solvents,[23,24] complexity largely increases in water, where hydrophobic effects play a fundamental role. This hinders experimental determination of the molecular factors controlling supramolecular polymerization.[21] For this reason, molecular simulations have recently emerged as a useful tool to gain molecular-level insight into supramolecular polymers in various media,[25–29] including water.[15,30–35]

Recently, we have reported atomistic molecular dynamics (AA-MD) simulations of BTA supramolecular polymers in explicit water, providing high-resolution (atomistic) details of the structure and order into these fibers.[30] We also unraveled the key types of interactions controlling these supramolecular polymers in water (H-bonding, hydrophobic effects, etc.), their

cooperativity and the amplification of order into the growing BTA fibers.[31] However, a major challenge (both in the experiments and simulations) is studying the dynamic self-assembly of these fibers while keeping a high resolution in the description of the monomers.

Starting from this detailed (atomistic) information, we have recently developed a transferable coarse-grained (CG) model for water-soluble BTA supramolecular polymers.[32] Based on the MARTINI force field,[36] this model also includes the possibility of an explicit treatment of inter-monomer H-bonding. This explicit-water BTA CG model was proven fully consistent with the AA ones, correctly reproducing the behavior of the BTA monomers in water, the strength and the cooperativity of all the key interactions (H-bonding, hydrophobic effects, etc.) involved in the self-assembly. While allowing us to study for the first time BTA supramolecular polymerization in water in time at high-resolution (submolecular), this model also demonstrated optimal agreement with the experiments, correctly capturing the effect of subtle changes in the surrounding conditions (temperature) or in the monomer structure, easily implementable thanks to the transferability guaranteed by the MARTINI force field, on supramolecular polymer structure[32] and dynamics.[35]

Despite these tremendous advantages, this CG model is still limited by the number of monomers that can be practically modeled using explicit water beads to represent the solvent. Another typical drawback of explicit solvent molecular models is that the simulated systems are unavoidably over-concentrated (in our case, ~2-3 orders of magnitude higher than in the experiments),[24] whereas decreasing even slightly the concentration into the models by reducing the number of monomers or enlarging the simulation box readily results into statistical irrelevance or a prohibitive computational cost for the simulations (high number of water particles to be simulated).

Herein, we present an implicit-solvent CG model for water-soluble BTA supramolecular polymers. Starting from our accurate explicit-solvent CG models for water-soluble BTAs, we adapted these to be compatible with the Dry MARTINI force field environment.[37] The implicit-solvent CG BTA models (Figure 1: DRY-BTA) were then refined to obtain the best possible agreement with the explicit-water CG[24] and AA[23] models for the same monomers. In particular, it was fundamental to verify that these were able to correctly capture the key factors controlling BTA self-assembly (supramolecular polymerization) in water – *i.e.*, monomer behavior in water, monomer-monomer interaction, cooperativity of the interactions involved in the self-assembly and order amplification during polymer growth.[32]

The implicit-solvent CG parameters for the BTA core (aromatic cores+amides) were opportunely tuned to obtain a dimerization free-energy profile consistent with those obtained using our explicit-solvent AA and CG models[32] (obtained via metadynamics[38] simulations, where two BTA cores+amides in implicit-solvent were let stacking/destacking multiple times – see SI). According to our explicit-water CG models for these BTAs, we built two variants of this implicit-solvent CG model – *i.e.*, one with (DRY-BTA_c) and one without (DRY-BTA_0) explicit treatment of inter-monomer H-bonding. To represent the amides, in DRY-BTA_0 we chose the Dry MARTINI beads giving the best matching in terms of dimerization free-energy profile with the explicit-water CG and AA models. On the other hand, as done previously,[32] in DRY-BTA_c we created a custom CG bead (Figure 1b: AMD_c) containing a rigidly rotating $\pm q$ dipole mimicking the rigid orientation in the amides and the directionality of H-bonding typical of the AA models. The value and distance between the $\pm q$ charges were optimized to reproduce the same dimerization free-energy (see SI). Both implicit-solvent models showed optimal agreement with the corresponding explicit-solvent CG and AA models (see SI: Figure S1). For the dodecyl

spacers, we used standard dry-SC1 beads, while for the PEG terminal units we used the Dry MARTINI parameters recently reported by Larsson *et al*.[39] All non-bond interactions used in the DRY-CG models are reported in the SI (Table S1), while the bond terms are the same of our previously reported explicit water CG-BTA model.[32]

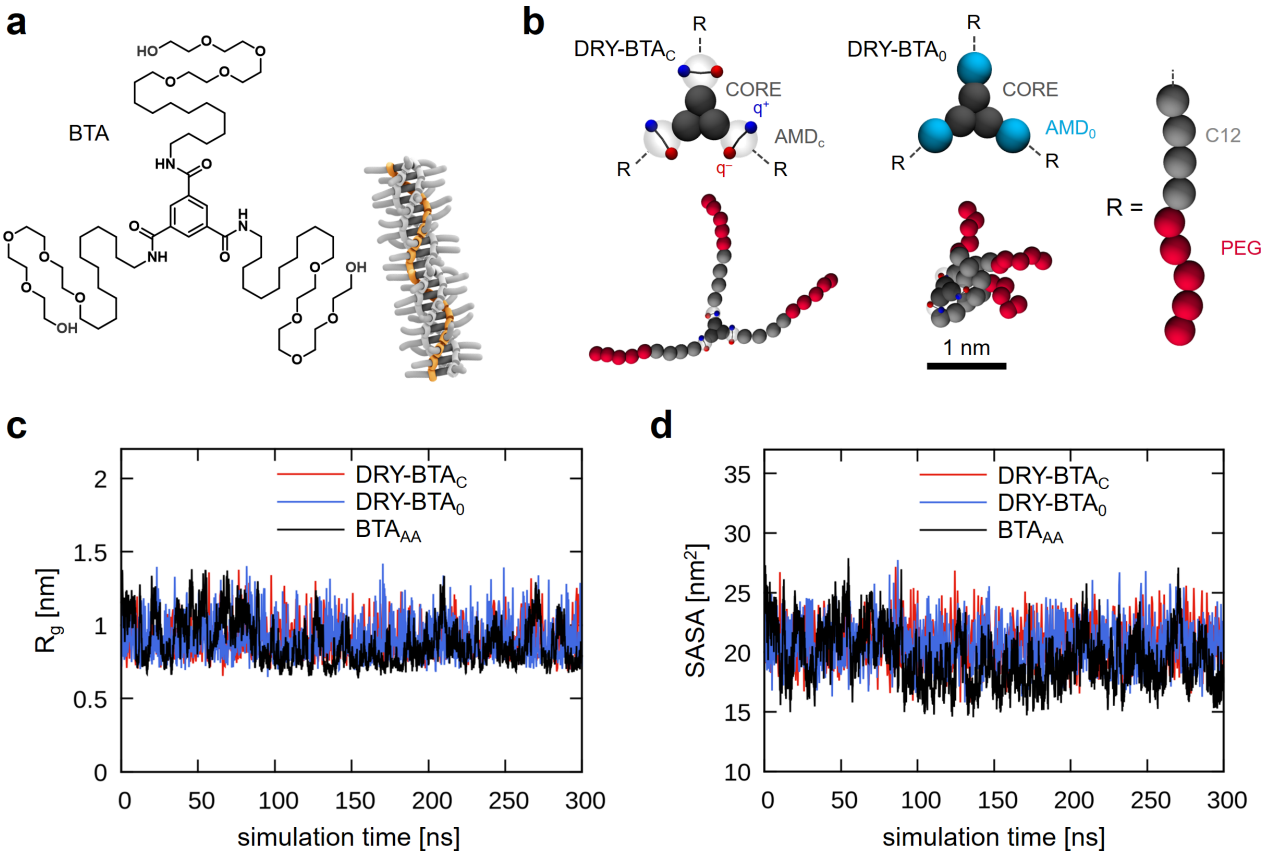

Figure 1. Implicit-solvent CG models for water-soluble BTA supramolecular polymers. (a) Chemical structure of water-soluble BTA monomers. (b) CG representation of the DRY-BTA core and side chains. DRY-BTA$_C$ and DRY-BTA$_0$ models differ only in the description of the amides (AMD$_c$ or AMD$_0$). (c,d) Behavior of the DRY-BTA monomers. Comparison of the (c) radius of gyration (R$_g$) and (d) solvent-accessible surface area (SASA) for the DRY-BTA$_C$ and DRY-BTA$_0$ monomers with the explicit-solvent AA model for the same monomer.[32]

The radius of gyration (R$_g$) and the solvent accessible surface area (SASA) for the DRY-BTA monomers were found optimally consistent with the AA models (Figure 1c,d), and nearly identical to the explicit-water CG-BTA models in water.[32] To measure the dimerization strength

of two full DRY-BTA monomers we used metadynamics simulations (see SI),[24] particularly useful in the study of complex/flexible polymeric systems.[40] For both DRY-BTA_c and DRY-BTA_0 we obtained a dimerization free-energy of -9±2 kcal mol^{-1}, identical to that previously obtained for explicit-water AA and CG-BTA models.[24] Thus, the DRY-BTA CG models demonstrated to correctly capture both the behavior of the individual monomer and of monomer-monomer interaction in solution.

A fundamental point for these supramolecular polymers is self-assembly cooperativity. To verify that these DRY-BTA models correctly capture the cooperativity in the key types of interactions involved in the self-assembly, we constructed and equilibrated pre-stacked DRY-BTA oligomers of different size (Figure 2: 2, 3, 5, 7, 14, 21 and 84DRY-BTA). We extracted information on H-bonding and the strength of hydrophobic interactions for all different size oligomers. Thanks to the advantages of this DRY-BTA model, we could easily simulate 1000 BTA monomers, which underwent self-assembly forming long fibers (Figure 3a). The data for these large systems are also added to the cooperativity plots of Figure 2. The relative shrinkage of the average monomer SASA in the oligomers (ΔSASA: calculated as the difference between the average SASA of the BTAs in the different size assemblies and that of the BTA monomer dissolved in solution) provides indication of the strength of the hydrophobic effects. Seen in Figure 2b (dotted lines), the ΔSASA becomes larger in absolute value while growing with the size of the assemblies, plateauing for the larger systems (both DRY-BTA_c and DRY-BTA_0 models show comparable cooperativity of hydrophobic effects, identical to that obtained with our explicit-water CG-BTA model).[32]

The explicit $\pm q$ charges in the amides of the DRY-BTA_c oligomers allow directly monitoring the number of H-bonds per-monomer into the system.[32] The average number and cooperativity of

H-bonding in the DRY-BTA$_c$ models (Figure 2b: red) are found substantially identical to those found using our explicit-solvent CG-[32] and AA-BTA models:[23] the number of equivalent H-bonds per-BTA is seen to increase from ~0.5 for the dimer to ~2.3 at saturation. Interestingly, properly tuning of the threshold distance for the calculation of the contacts between the amide CG beads (see SI) allows obtaining an equivalent data for implicit H-bonding also with the DRY-BTA$_0$ model (Figure 2b: blue).

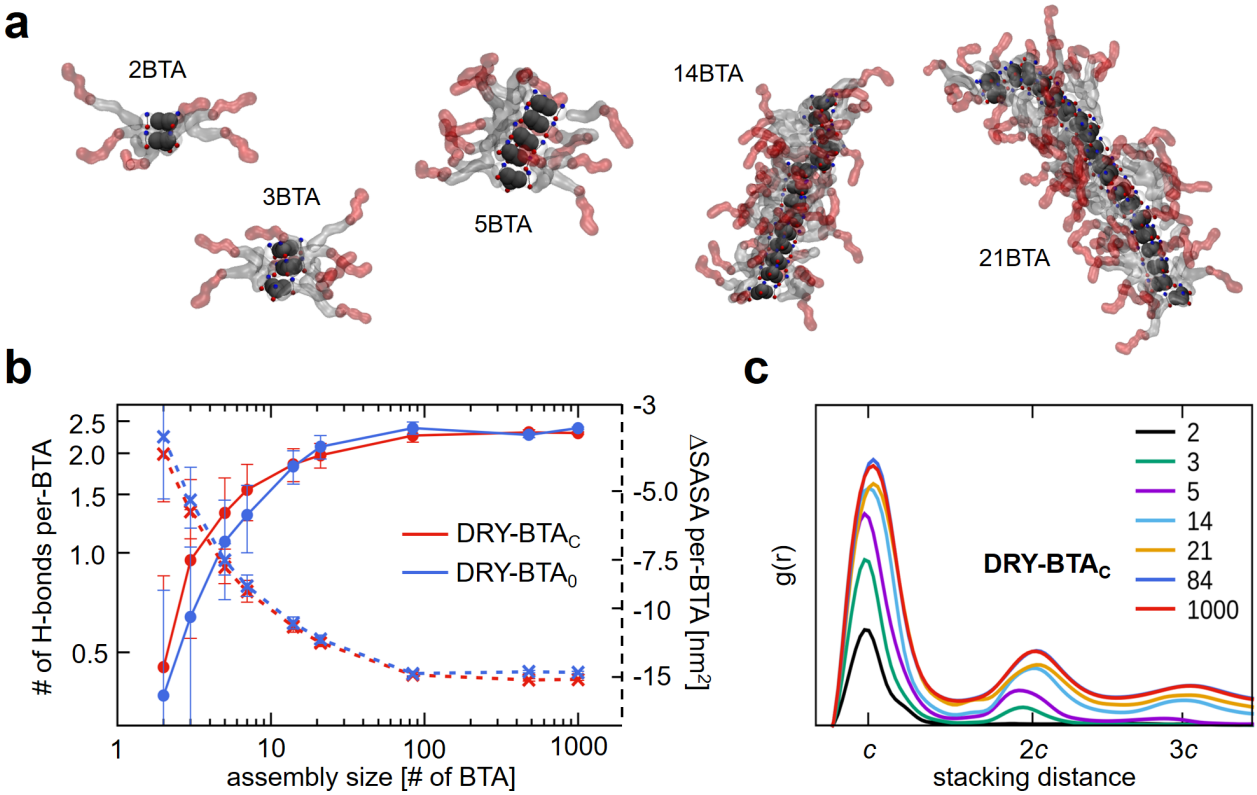

Figure 2. Self-assembly cooperativity and amplification of order during growth captured by the DRY-BTA models. (a) Hydrophobic effect: SASA variation (ΔSASA) per-BTA as a function of the size of the BTA oligomers. (b) Average number of equivalent H-bonds per-BTA as a function of the size. (c,d) Radial distribution functions *g(r)* of the BTA cores for the different size assemblies, in the two model variants respectively (DRY-BTA$_C$ and DRY-BTA$_0$). Amplification of stacking order into the growing BTA oligomers is demonstrated by the increasing height of the *g(r)* peaks at stacking distance *c*, 2*c*, 3*c* (fist, second, third neighbor).

The evolution of the *g(r)* of the BTA cores into the growing size DRY-BTA stacks is a good indicator of the amplification of the stacking order in the supramolecular polymer – the higher

the *g(r)* peaks at stacking distance *c*, 2*c*, 3*c* (first, second, third neighbor), the higher the persistency of the core stacking into the assembly. The height of the *g(r)* peaks increases with the size of the BTA_C assemblies, reaching saturation in the largest systems (Figure 2c). This amplification of order during fiber growth is again consistent with what recently observed in the explicit-water AA[31] and CG-BTA[32] models. In summary, all extracted parameters demonstrate that these DRY-BTA models can also correctly capture the cooperativity of self-assembly and the amplification of order during supramolecular polymerization, proving that their accuracy is fully comparable to that of explicit-water CG models and the AA ones for the study of these water-soluble BTA fibers and their supramolecular polymerization.

The main advantages of these DRY-BTA models consists in the possibility to simulate a larger number of monomers and to freely increase the size of the simulation box for simulating very dilute systems (too computationally demanding for explicit-solvent models). This allows studying the effect of concentration on the polymerization mechanism. We started from a reference system (Figure 3a) containing 1000 dissolved DRY-BTA_c monomers randomly placed into a cubic simulation box with sides of 30x30x30 nm, corresponding to a concentration of ~48 mM (complete computational details are provided in the SI). After 7.5 μs of simulation, the DRY-BTA_c monomers had spontaneously formed very long fibers (~50 nm of length). It is interesting to monitor both the evolution of the average size and of stacking order into the assemblies (measured by the order parameter, Φ: average coordination between the BTA cores) during the polymerization process. As previously seen using our explicit-water CG models,[32] the BTA monomers aggregate very fast (abrupt decrease in the number of clusters present in the system – Figure 3b: dotted lines), while the ordering of the aggregates (growth of Φ, solid lines)

proceeds on a slower timescale (see also SI – Figure S2 for a self-assembly free energy landscape).

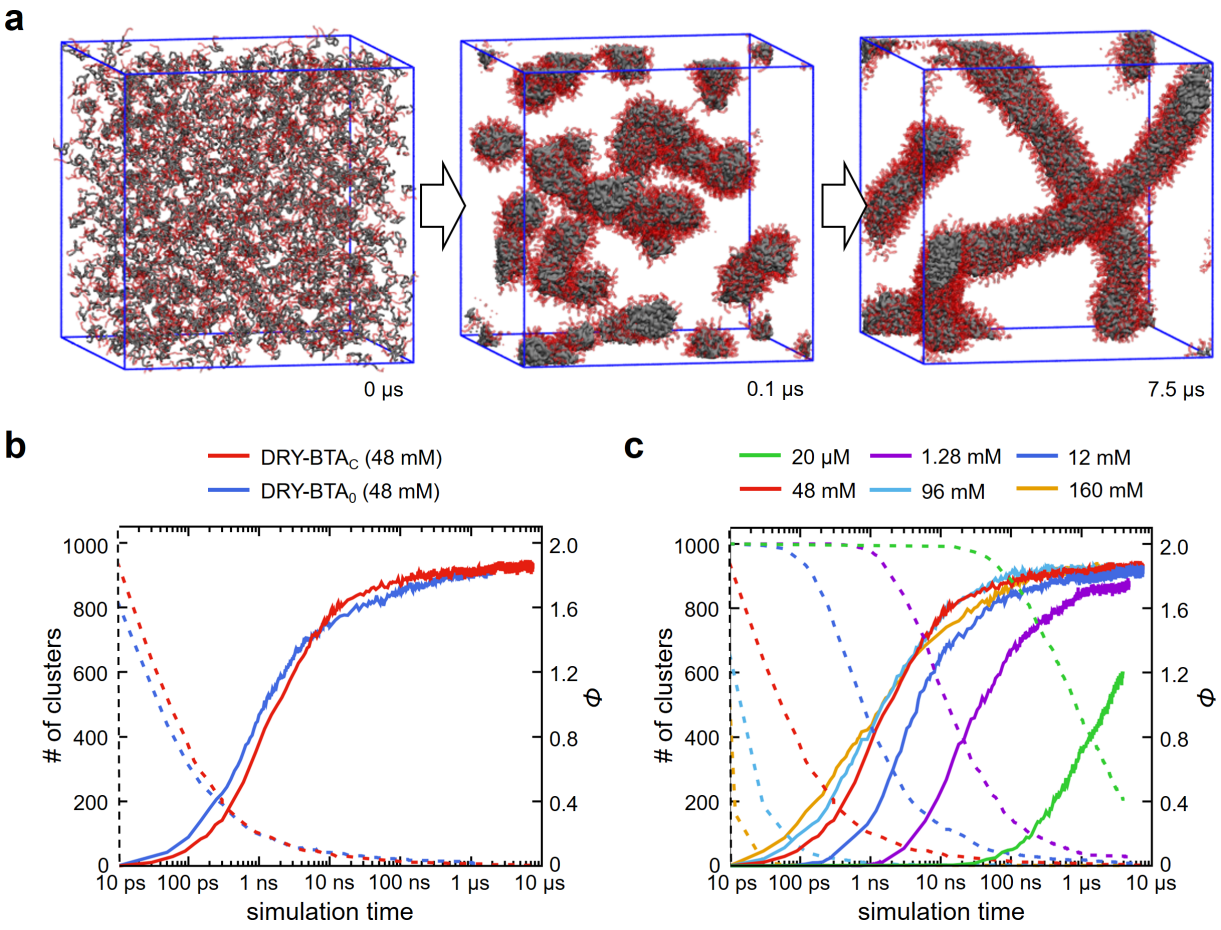

Figure 3. Self-assembly and polymerization of a 1000 BTA monomers. (a) Snapshots taken at three different times from the simulation with the BTA_C model at a concentration of 48 mM. (b) Number of BTA clusters and order parameter Φ (core-core coordination) as a function of time for both BTA_C and BTA_0 models at 48mM. (c) Number of BTA clusters and order parameter Φ (core-core coordination) as a function of time for the BTA_C model at six molar concentrations.

It is extremely interesting to study how these two key phases (growth and ordering) in the polymerization mechanism change when the monomer concentration in solution is changed. In fact, we have already observed using our explicit-solvent CG model that the polymerization mechanism can be influenced, to some extent, by the BTA molar concentration in solution.[32] We systematically changed the box size while keeping constant the number of monomers in the

systems. We came out with two higher-concentration systems (96 mM and 160 mM respectively) to compare with our reference 48 mM system, and three more diluted ones (12 mM, 1.28 mM and 20 μM). The last, most diluted system (20 μM) is in the same range of the typical concentrations used in the experiments.[30,31] Such a condition could be modeled only thanks to the notable computation advantages provided by our DRY-BTA model. In fact, it is worth considering that such a dilute concentration, obtained enlarging the box sides up to 400x400x400 nm, would correspond to >1.6 billions of water molecules into the system (>400 millions of water CG beads in the explicit-solvent MARTINI environment)!

Figure 3c shows the same data for all 6 simulated concentrations. For what concerns the self-assembly rate, the effect of increasing the dilution is clearly visible from the shift to the right (longer simulation times) of the dotted curves representing the decrease in the number of clusters in solution (fusion of the aggregates). Interestingly, increasing the concentration into the system produces a speed-up in the ordering of the assemblies (Φ: solid lines) only up to a certain concentration (48 mM). Over this threshold, this proceeds at the same rate also for the higher concentrations (96 mM and 160 mM). This means that there is a physical limit in the velocity of the reorganization of the assemblies to optimize the interactions that is independent on the concentration in solution (at least above a certain concentration value).

A convenient way to represent the polymerization mechanism is plotting the order parameter Φ against the average cluster size (Figure 4). The red curve (48 mM) shows the same sigmoidal behavior observed in our previous work.[24] This means that the DRY-BTA$_c$ monomers first self-assemble into disordered aggregates, but then, instead of growing further in disordered way, the system proceeds toward ordered oligomers. Fiber growth then proceeds via the fusion of these stacked oligomers. When moving to higher monomer concentrations, the curves change tending

to an "L" shape (Figure 4: yellow). This occurs because at such high concentrations the initial aggregation is so fast (Figure 3c: dotted yellow curve) that monomers rapidly form a few (or a single) large cluster before having the possibility to order. Ordering then proceeds once the average cluster size is already large, or has even reached the maximum limit (1000, 1 single cluster in the system). On longer timescales, such highly concentrated systems form fibers inter-connected to each other through the PBC box (a gel-like structure, see SI: Figure S3).

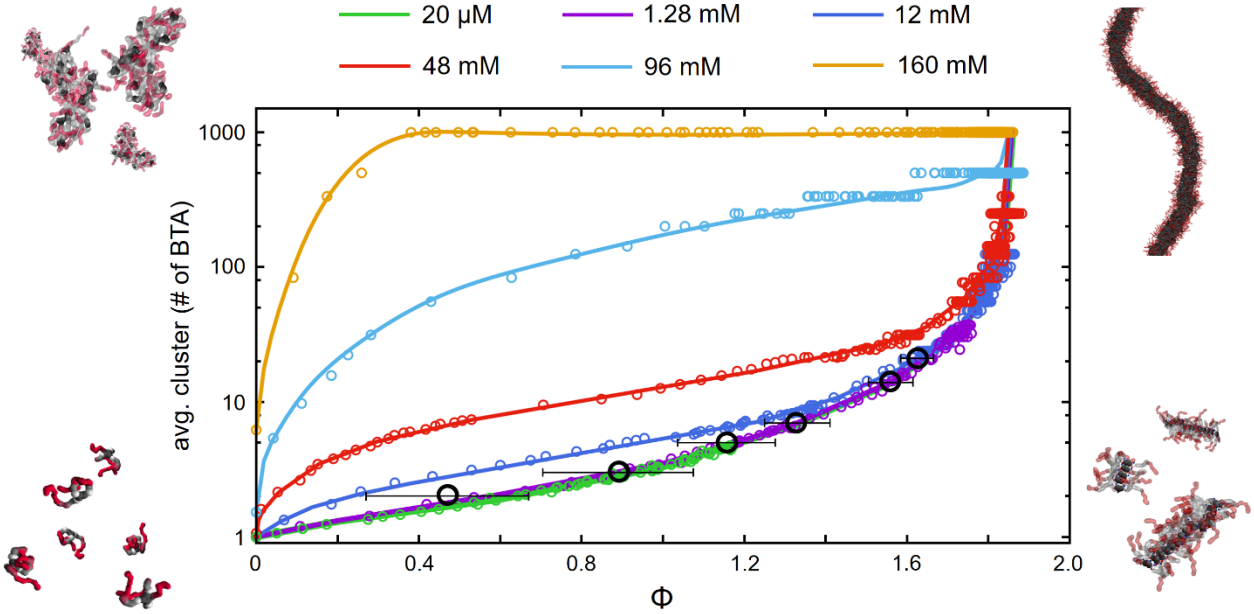

Figure 4. Mechanism of BTA supramolecular polymerization as a function of monomer concentrations. Colored lines guide the eye through the simulation data obtained for each system at different concentrations. Black points represent the average order (Φ, with standard deviations) into the prestacked oligomers (2, 3, 5, 7, 14 and 21DRY-BTA$_c$) at the thermodynamic equilibrium.

More interesting is what happens when decreasing the concentration in the systems. Below 12 mM, the curves tend toward a reverse "L" shape. Interestingly, the curves for the two lowest concentrations (1.28 mM and 20 μM) are perfectly superimposed, while in the latter case the growth of large aggregates becomes extremely slow (large distance between the formed oligomers into the box). Shown in Figure 4, the curves for these two dilute cases follow a well-

defined path identified by black points. The latters represent the data extracted from the pre-formed DRY-BTA$_c$ stacks of Figure 2 (2, 3, 5, 7, 14, 21DRY-BTA$_c$) used for the study of cooperativity, from which we calculated the order parameter (Φ) at the equilibrium. This means that in our model at 1.28 mM we are already in the same condition of the most dilute 20 μM concentration, where kinetic effects on the polymerization mechanism due to monomer over-concentration have disappeared.

In conclusions, we have developed an accurate implicit-solvent CG model for a water-soluble BTA supramolecular polymer. This is consistent with the explicit-water models (AA and CG) for all key features controlling these supramolecular polymers, it allows simulating the self-assembly of long fibers and to study the mechanism of supramolecular polymerization in water. We can study a large number of monomers in a wide range of experimentally relevant conditions, obtaining unique insight into the effect of concentration on the polymerization mechanism. We observe that below a certain threshold, the BTA concentration does not influence the mechanism of polymerization, while above this threshold the kinetic effects start playing an important role. Based on the Dry MARTINI force field, this model can be in principle adapted to other BTA variants, opening the way to the study of the effect of molecular structure on the polymerization mechanism, and the intriguing possibility of modeling the interaction of these fibers with large biorelevant supramolecular targets (*e.g.*, lipid bilayers, etc.).

ASSOCIATED CONTENT

Supporting Information. Complete computational methods and procedures, additional data from the molecular simulations. The following files are available free of charge (Supporting_Information.pdf).

AUTHOR INFORMATION

Corresponding Author

*Giovanni M. Pavan. Department of Innovative Technologies, University of Applied Sciences and Arts of Southern Switzerland, Galleria 2, Via Cantonale 2c, CH-6928 Manno, Switzerland. Email: giovanni.pavan@supsi.ch

ACKNOWLEDGMENT

The authors acknowledge the support from the Swiss National Science Foundation (SNSF grant 200021_162827 to GMP).

REFERENCES

(1) Aida, T.; Meijer, E. W.; Stupp, S. I. Functional Supramolecular Polymers. *Science* **2012**, *335* (6070), 813–817.

(2) Krieg, E.; Bastings, M. M. C.; Besenius, P.; Rybtchinski, B. Supramolecular Polymers in Aqueous Media. *Chem. Rev.* **2016**, *16* (4), 2414–2477.

(3) Webber, M. J.; Appel, E. A.; Meijer, E. W.; Langer, R. Supramolecular Biomaterials. *Nat. Mater.* **2015**, *15* (1), 13–26.

(4) Yang, L.; Tan, X.; Wang, Z.; Zhang, X. Supramolecular Polymers: Historical Development, Preparation, Characterization, and Functions. *Chem. Rev.* **2015**, *115* (15), 7196–7239.

(5) Lehn, J.-M. Dynamers: Dynamic Molecular and Supramolecular Polymers. *Prog. Polym. Sci.* **2005**, *30* (8–9), 814–831.

(6) Davis, A. V; Yeh, R. M.; Raymond, K. N. Supramolecular Assembly Dynamics. *Proc. Natl. Acad. Sci.* **2002**, *99* (8), 4793–4796.

(7) da Silva, R. M. P.; van der Zwaag, D.; Albertazzi, L.; Lee, S. S.; Meijer, E. W.; Stupp, S. I. Super-Resolution Microscopy Reveals Structural Diversity in Molecular Exchange among Peptide Amphiphile Nanofibres. *Nat. Commun.* **2016**, *7*, 11561.

(8) Yan, X.; Wang, F.; Zheng, B.; Huang, F. Stimuli-Responsive Supramolecular Polymeric Materials. *Chem. Soc. Rev.* **2012**, *41* (18), 6042.

(9) Appel, E. A.; Loh, X. J.; Jones, S. T.; Biedermann, F.; Dreiss, C. A.; Scherman, O. A. Ultrahigh-Water-Content Supramolecular Hydrogels Exhibiting Multistimuli Responsiveness. *J. Am. Chem. Soc.* **2012**, *134* (28), 11767–11773.

(10) Bastings, M. M. C.; Koudstaal, S.; Kieltyka, R. E.; Nakano, Y.; Pape, A. C. H.; Feyen, D. A. M.; van Slochteren, F. J.; Doevendans, P. A.; Sluijter, J. P. G.; Meijer, E. W.; et al. A Fast pH-Switchable and Self-Healing Supramolecular Hydrogel Carrier for Guided, Local Catheter Injection in the Infarcted Myocardium. *Adv. Healthc. Mater.* **2014**, *3* (1), 70–78.

(11) Matson, J. B.; Zha, R. H.; Stupp, S. I. Peptide Self-Assembly for Crafting Functional Biological Materials. *Curr. Opin. Solid State Mater. Sci.* **2011**, *15* (6), 225–235.

(12) Dankers, P. Y. W.; Harmsen, M. C.; Brouwer, L. A.; Van Luyn, M. J. A.; Meijer, E. W. A Modular and Supramolecular Approach to Bioactive Scaffolds for Tissue Engineering. *Nat. Mater.* **2005**, *4* (7), 568–574.

(13) Cui, H.; Webber, M. J.; Stupp, S. I. Self-Assembly of Peptide Amphiphiles: From Molecules to Nanostructures to Biomaterials. *Biopolymers* **2010**, *94* (1), 1–18.

(14) Fukui, T.; Kawai, S.; Fujinuma, S.; Matsushita, Y.; Yasuda, T.; Sakurai, T.; Seki, S.; Takeuchi, M.; Sugiyasu, K. Control over Differentiation of a Metastable Supramolecular Assembly in One and Two Dimensions. *Nat. Chem.* **2016**, *9* (5), 493–499.

(15) Garzoni, M.; Cheval, N.; Fahmi, A.; Danani, A.; Pavan, G. M. Ion-Selective Controlled Assembly of Dendrimer-Based Functional Nanofibers and Their Ionic-Competitive Disassembly. *J. Am. Chem. Soc.* **2012**, *134* (7), 3349–3357.

(16) Li, J.; Loh, X. J. Cyclodextrin-Based Supramolecular Architectures: Syntheses, Structures, and Applications for Drug and Gene Delivery. *Adv. Drug Deliv. Rev.* **2008**, *60* (9), 1000–1017.

(17) Neirynck, P.; Brinkmann, J.; An, Q.; van der Schaft, D. W. J.; Milroy, L.-G.; Jonkheijm, P.; Brunsveld, L. Supramolecular Control of Cell Adhesion via Ferrocene-cucurbit[7]uril Host-Guest Binding on Gold Surfaces. *Chem. Commun.* **2013**, *49* (35), 3679–3681.

(18) Wang, J.; Xia, H.; Zhang, Y.; Lu, H.; Kamat, R.; Dobrynin, A. V.; Cheng, J.; Lin, Y. Nucleation-Controlled Polymerization of Nanoparticles into Supramolecular Structures. *J. Am. Chem. Soc.* **2013**, *135* (31), 11417–11420.

(19) Cantekin, S.; de Greef, T. F. A.; Palmans, A. R. A. Benzene-1,3,5-Tricarboxamide: A Versatile Ordering Moiety for Supramolecular Chemistry. *Chem. Soc. Rev.* **2012**, *41* (18), 6125–6137.

(20) Leenders, C. M. A.; Baker, M. B.; Pijpers, I. A. B.; Lafleur, R. P. M.; Albertazzi, L.; Palmans, A. R. A.; Meijer, E. W. Supramolecular Polymerisation in Water; Elucidating the Role of Hydrophobic and Hydrogen-Bond Interactions. *Soft Matter* **2016**, *12* (11),

2887–2893.

(21) Leenders, C. M. A.; Albertazzi, L.; Mes, T.; Koenigs, M. M. E.; Palmans, A. R. A.; Meijer, E. W. Supramolecular Polymerization in Water Harnessing Both Hydrophobic Effects and Hydrogen Bond Formation. *Chem. Commun.* **2013**, *49* (19), 1963–1965.

(22) Albertazzi, L.; van der Zwaag, D.; Leenders, C. M. A.; Fitzner, R.; van der Hofstad, R. W.; Meijer, E. W. Probing Exchange Pathways in One-Dimensional Aggregates with Super-Resolution Microscopy. *Science* **2014**, *344* (6183), 491–495.

(23) Korevaar, P. A.; George, S. J.; Markvoort, A. J.; Smulders, M. M. J.; Hilbers, P. A. J.; Schenning, A. P. H. J.; De Greef, T. F. A.; Meijer, E. W. Pathway Complexity in Supramolecular Polymerization. *Nature* **2012**, *481* (7382), 492–496.

(24) Korevaar, P. A.; De Greef, T. F. A.; Meijer, E. W. Pathway Complexity in π-Conjugated Materials. *Chemistry of Materials* **2014**, *26*, 576–586.

(25) Bejagam, K. K.; Fiorin, G.; Klein, M. L.; Balasubramanian, S. Supramolecular Polymerization of Benzene-1,3,5-Tricarboxamide: A Molecular Dynamics Simulation Study. *J. Phys. Chem. B* **2014**, *118* (19), 5218–5228.

(26) Kulkarni, C.; Bejagam, K. K.; Senanayak, S. P.; Narayan, K. S.; Balasubramanian, S.; George, S. J. Dipole-Moment-Driven Cooperative Supramolecular Polymerization. *J. Am. Chem. Soc.* **2015**, *137* (11), 3924–3932.

(27) Bejagam, K. K.; Balasubramanian, S. Supramolecular Polymerization: A Coarse Grained Molecular Dynamics Study. *J. Phys. Chem. B* **2015**, *119* (17), 5738–5746.

(28) Albuquerque, R. Q.; Timme, A.; Kress, R.; Senker, J.; Schmidt, H. W. Theoretical Investigation of Macrodipoles in Supramolecular Columnar Stackings. *Chem. - A Eur. J.* **2013**, *19* (5), 1647–1657.

(29) Filot, I. A. W.; Palmans, A. R. A.; Hilbers, P. A. J.; Van Santen, R. A.; Pidko, E. A.; De Greef, T. F. A. Understanding Cooperativity in Hydrogen-Bond-Induced Supramolecular Polymerization: A Density Functional Theory Study. *J. Phys. Chem. B* **2010**, *114* (43), 13667–13674.

(30) Baker, M. B.; Albertazzi, L.; Voets, I. K.; Leenders, C. M. a; Palmans, A. R. a; Pavan, G. M.; Meijer, E. W. Consequences of Chirality on the Dynamics of a Water-Soluble Supramolecular Polymer. *Nat. Commun.* **2015**, *6*, 6234.

(31) Garzoni, M.; Baker, M. B.; Leenders, C. M. A.; Voets, I. K.; Albertazzi, L.; Palmans, A. R. A.; Meijer, E. W.; Pavan, G. M. Effect of H-Bonding on Order Amplification in the Growth of a Supramolecular Polymer in Water. *J. Am. Chem. Soc.* **2016**, *138* (42), 13985–13995.

(32) Bochicchio, D.; Pavan, G. M. From Cooperative Self-Assembly to Water-Soluble Supramolecular Polymers Using Coarse-Grained Simulations. *ACS Nano* **2017**, *11* (1), 1000–1011.

(33) Lee, O. S.; Stupp, S. I.; Schatz, G. C. Atomistic Molecular Dynamics Simulations of Peptide Amphiphile Self-Assembly into Cylindrical Nanofibers. *J. Am. Chem. Soc.* **2011**, *133* (10), 3677–3683.

(34) Lee, O. S.; Cho, V.; Schatz, G. C. Modeling the Self-Assembly of Peptide Amphiphiles

into Fibers Using Coarse-Grained Molecular Dynamics. *Nano Lett*. **2012**, *12* (9), 4907–4913.

(35) Bochicchio, D.; Salvalaglio, M.; Pavan, G. M. Into the Dynamics of a Supramolecular Polymer at Submolecular Resolution. *Nat. Commun*. **2017**, DOI: 10.1038/s41467-017-00189-0.

(36) Marrink, S. J.; Risselada, H. J.; Yefimov, S.; Tieleman, D. P.; De Vries, A. H. The MARTINI Force Field: Coarse Grained Model for Biomolecular Simulations. *J. Phys. Chem. B* **2007**, *111* (27), 7812–7824.

(37) Arnarez, C.; Uusitalo, J. J.; Masman, M. F.; Ingólfsson, H. I.; De Jong, D. H.; Melo, M. N.; Periole, X.; De Vries, A. H.; Marrink, S. J. Dry Martini, a Coarse-Grained Force Field for Lipid Membrane Simulations with Implicit Solvent. *J. Chem. Theory Comput*. **2015**, *11* (1), 260–275.

(38) Laio, A.; Parrinello, M. Escaping Free-Energy Minima. *Proc. Natl. Acad. Sci. U. S. A*. **2002**, *99* (20), 12562–12566.

(39) Wang, S.; Larson, R. G. A Coarse-Grained Implicit Solvent Model for Poly(ethylene Oxide), CnEm Surfactants, and Hydrophobically End-Capped Poly(ethylene Oxide) and Its Application to Micelle Self-Assembly and Phase Behavior. *Macromolecules* **2015**, *48* (20), 7709–7718.

(40) Pavan, G. M.; Barducci, A.; Albertazzi, L.; Parrinello, M. Combining Metadynamics Simulation and Experiments to Characterize Dendrimers in Solution. *Soft Matter* **2013**, *9* (9), 2593.